RSC Advances

ROYAL SOCIETY OF CHEMISTRY

www.rsc.org/advances

Strain and structure order variation of pure aluminum due to helium irradiation

Hao Wan[1], Naichao Si[1], Kangmin Chen[1], Quan Wang[2, 3] *

1. *School of Materials Science and Engineering , Jiangsu University, Zhengjiang212013, RP China*

2. *School of Mechanical Engineering , Jiangsu University, Zhengjiang212013, RP China*

3. *State Key Laboratory of Transducer Technology, Chinese Academy of Sciences, Shanghai 200050, P.R.China*

Abstract

Mechanisms were proposed to interpret strain changes and phases transformation caused by ordering crystal structure broken in He^+ irradiation 1060 pure aluminum.

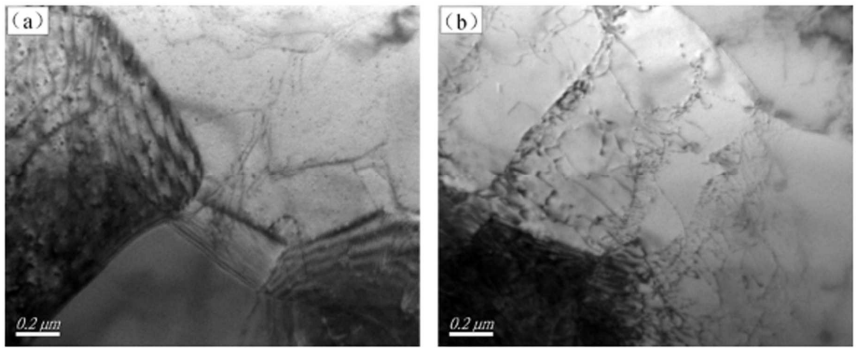

*Author to whom correspondence should be addressed. Electronic mail: wangq@mail.ujs.edu.cn

Strain and structure order variation of pure aluminum due to helium irradiation

Hao Wan[1], Naichao Si[1], Kangmin Chen[1], Quan Wang[2, 3] *

1. *School of Materials Science and Engineering , Jiangsu University, Zhengjiang212013, RP China*

2. *School of Mechanical Engineering , Jiangsu University, Zhengjiang212013, RP China*

3. *State Key Laboratory of Transducer Technology, Chinese Academy of Sciences, Shanghai 200050, PR China*

Abstract

Damages induecd by helium ion irradiation in 1060 pure aluminum was investigated with a home-made MT3-R ion implanter. In this process, 10^{15}, 10^{16} and 10^{17} ions/cm^2 irradiation was carried out with 50 kV voltage, respectively. In order to evaluate irriadiation damages in samples, surface morphology changes, strain variation and microstructure transformation have been examined using scanning electron microscope (SEM), atomic force microscopy (AFM), X-Ray diffraction (XRD) and transmission electron microscopy (TEM). Besides, detail collision events of energetic ions with target atoms were simulated using SRIM-2008. The result shows that, irradiation dose plays the most important role in changing target surface layer. Increasing irradiation dose further damaged surface layer morphology and increased surface roughness. In this process, strain changes and phases transformation caused by ordering crystal structure broken were discussed and mechanism was proposed to explain the phenomenon appeared at different irradiation stage. In addition, variation of dislocations observed by TEM confirmed this conclusion.

*Author to whom correspondence should be addressed. Electronic mail: wangq@mail.ujs.edu.cn

1 Introduction

In recent years, ion irradiation technique has become a novel method in the field of material processing, as well as being relevant to radiation damage occurred in nuclear protection material and aeronautical material. When energetic ions impinge on sample surface, ions with several tens of keV or higher energies can be implanted.[1] As a result of momentum transfer between incident ions and target atoms, some damages would be induced in sample surface. Earlier research revealed various energetic ions caused defects on different materials, including micro-cracks, bubbles, blisters, pinholes, crystal damage, etc.[2,3,4,5,6] In order to examine characteristic changes of irradiated samples, some experiments have been conducted.[7,8,9,10] Li *et al.*[7] used micro-compression test to study the effect of nanometer-scale helium bubble on strength and deformability of sputter-deposited Cu and Cu/Nb multi-layers. Cui *et al.*[8] observed interaction between lattice dislocations and grain boundaries in austenitic stainless by in situ transmission electron microscopy (TEM). Aabdin *et al.*[9] performed argon ions irradiation to switch natural nanostructure ON and OFF in Bi_2Ti_3 materials. Xiao *et al.*[10] transformed amorphization silicon into polycrystalline silicon after gallium implantation by annealing treatment, which provided sufficient energy for recrystallization.

Moreover, with energetic ions bombardment of target surface, secondary electrons and secondary ions generated at the surface are utilized to form high resolution images.[11] In addition, surface or near-surface atoms of target can get rid of surface binding energy when they receive sufficient momentum from incident ions,

which was employed to modify or mill micro and nanometer scale structural shape of target precisely. For instance, by setting ion-projected range and angle of incidence ion beam, Romero-Gomez et al.[12] found that well-ordered nanorods appear in TiO_2 film surface layer. Nanovoid structure was observed in Ar^+ implanted GaSb wafer,[13] a similar phenomenon was found in N+ irradiated TiO_2 film.[1] Besides, nanocavities were found in He^+ irradated Si and Ge.[14] Nano-strings, nano-bead chains and nano-pore membranes were fabricated with smooth surfaces using focused ion beam technique.[15]

As an alloy with low density and high strength, pure aluminum was commonly employed as anti-radiation material of aircraft, which always expose to the radiation of energetic charged particle current in the space, such as solar wind[16] (during a period of solar minium, the flux of He^+ is $10^3/cm^2$-day, most particles at energies of tens to hundreds of keV[17]). Current research focuses on the modification of aluminum alloys with heavy ions irradiation,[18, 19, 20] and the research of irradiation damage is rather little. Under current conditions, it is convenient to produce particles with tens of keV range perpendicular to the target surface. Moreover, light particles with several tens of keV constitute a major part of light particles in the space radiation environment. Hence, it is reasonable to choose 50kV as an acceleration voltage combines with the device and application. The main purpose of this work was to generate accelerated and energetic ions to simulate energetic charged particles (tens of keV range) via a home-made ion irradiation system. By varying irradiation time, helium ions with different doses were implanted to the surface layer of 1060 pure

aluminum. The relevant strain variation and order degree of sample structure were demonstrated, and these findings provide keen insights into durability and safety use of anti-radiation materials in space radiation.

2 Experimental

A 1 mm thickness rolling commercial 1060 pure aluminum sheet was selected as target material and the composition is shown in Table 1. Specimens were obtained by a wire-electrode cutting with a size 10×10×1 mm. Scanning electron microscope (SEM) samples were polished with diamond spray polishing compounds until ground up to a mesh number of 1000 by SiC sandpapers. TEM thin foils were prepared from sample surface layer. Firstly, the sample was grounded from undersurface to a plate with thickness less than 30 μm. After that, the plate was thinned in a Gatan-691 precision ion polishing system to electron transparency occurred, and a depth of sample surface layer was analyzed between 0.2 to 0.5 μm.

Irradiation experiment was carried out in a home-made MT3-R ion implanter, using helium ions oriented perpendicular implanted to surface of the samples. The schematic diagram of MT3-R ion implanter was shown in Fig. 1. During irradiation, a 10 μA/cm^2 beam current was produced using 50 kV acceleration voltage in a vacuum, which maintained a base pressure 10^{-4} Pa. In order to reach implantation dose 10^{15}, 10^{16} and 10^{17} ions/cm^2, dwell time of 22 s, 136 s and 1620 s were proceeded in 10×10 mm^2 specimens, respectively.

After that, morphologies of samples before and after irradiation were observed

using a Hitachi S3400 SEM. Roughness of sample surfaces was measured using a MFP-3D atom forced microscope (AFM). Strain and phase analyses were carried out employing a X-Ray diffraction (XRD) system, which performed between 15° to 90° (2θ) at room temperature with a step size of 0.02°. And the evaluation of dislocations in samples before and after irradiation was studied in a JOEL JEM-2100F TEM. Dislocation density was estimated by the line intercept method,[21] and the value was calculated by the following equation

$$\rho = \frac{2N}{Lt} \quad (1)$$

where ρ is dislocation density, L is the length of randomly drawn lines on the TEM image, N is the number of intersections(drawn lines with dislocations), and t is the foil thickness.

3 Results and discussion

Before experiment, simulation was performed on a SRIM-2008 software. SRIM is a software using Monte Carlo method to calculate ions distribution and defects generated by incident ions in target surface layer.[22] A stopping and range calculation predicts that, with 50 kV accelerating voltage, the peak concentration of energetic ions appear at 3405 angstroms beneath the target surface, and the distribution is in agreement with the Gaussian. Namely, incident ions tend to aggregate at a special depth R_0 (here, 3405 angstroms), and this tendency can be described as a Gaussian form

$$\rho(R) = \frac{1}{\Delta R_p \sqrt{2\pi}} exp - \frac{(R-R_0)^2}{2\Delta {R_P}^2} \quad (2)$$

where R is the depth of one incident ion stays, ΔR_p is the longitudinal straggling (815 angstroms, the value is given by SRIM, which is equivalent to standard deviation of the Gaussian[23]). In which, when incident ions travel in a solid matter, the energetic ions lose their energy through electronic and nuclear collision process. In SRIM, the energy loss was divided into ionization, vacancies and phonons by ions or recoils, as shown in table 2. In addition, crystal lattice defects were created in this process and the calculation results were illustrated in Fig. 2. The plot shows a number of 98 target atom displacements made by per incident ions, and these displacements give rise to either a target vacancy or a replacements collision. In this case, a number of 93 target vacancies and 4 replacement collisions were created.

Fig. 3 shows surface morphologies of reference samples and samples with 10^{15} ions/cm^2, 10^{16} ions/cm^2 and 10^{17} ions/cm^2 irradiation, respectively. According to a ternary Al-Fe-Si system, 1060 pure aluminum is made up of aluminum matrix, Al-Fe phases and Al-Fe-Si phases.[24] Fig. 3(a) illustrates the reference sample composed of aluminum matrix, and precipitate phases. Besides, due to the peeling of particles, trails formed in polishing process were also observed. When energetic helium ions bombarded the sample surface perpendicularly, pinholes and micro-cracks (the density is about 10^5/cm^2) began to appear on the sample surfaces, whereas precipitate phases disappeared partially, as depicted in Fig. 3(b). In Fig. 3(c), the pinholes (the density is about 10^5/cm^2) became deeper and bigger, while precipitate phases basically disappeared. This phenomenon aggravated with 10^{17} ions/cm^2 irradiation, as shown in Fig. 3(d). Therefore, rules can be found that deeper and bigger pinholes (the

density is about 5×10^5/cm^2) appeared and micro-cracks extended, but precipitate phases disappeared gradually with addition of irradiation dose. According to the above results, ion dose was confirmed as a major effect factor, having a great impact on defects formation and phase transformation[25] in target surface layer.

In order to study more details of surface morphology before and after helium irradiation, average roughness R_a of the samples was measured by AFM respectively, as illustrated in Fig. 4. The average roughness of reference sample is 3.235 nm, and a rising tendency was found after irradiation. With 10^{15} ions/cm^2, 10^{16} ions/cm^2 and 10^{17} ions/cm^2 irradiation, the average roughness turned to 3.633 nm, 5.516 nm and 6.178 nm, respectively. In addition, the absolute values of maximum and minimum roughness of the samples presented similar tendency. The increased roughness of sample surface may be due to the sputtering effect in crystal of ion irradiation.[26]

X-ray diffraction patterns of reference and the irradiation samples are shown in Fig. 5. The diffraction peaks correspond to aluminum matrix with face-centered cubic crystal structure (PDF#04-0787). Sharp peaks at 2θ equal to 38.472°, 44.738°, 65.133° and 78.227° appeared in the spectrum of reference sample are recognized as (111), (200), (220) and (311) planes, and these peaks can also be observed in the samples with different irradiation dose respectively. However, in comparison with reference sample, with 10^{15} ions/cm^2 helium ions irradiation, four peaks of α-Al phase appear at higher Bragg angles. But the deviation angle became lower with one order of magnitude added of irradiation ions (10^{16} ions/cm^2). When irradiation dose was increased to 10^{17} ions/cm^2, these peaks get shifted toward higher Bragg angles again.

Based on the XRD results and Bragg equation, interlayer spacing of (220) planes was calculated. The interlayer spacing of reference sample and samples with 10^{15} ions/cm^2, 10^{16} ions/cm^2 and 10^{17} ions/cm^2 irradiation are 286.1 Å, 285.6 Å, 286.9 Å, 285.4 Å respectively.

Indeed, when energetic helium ions are introduced into aluminum, energetic incident ions underwent a series of energy loss collisions with both electronic collisions and nuclear collisions, which generated target surface layer defects, such as interstitial atoms, replacement atoms, vacancies and lattice distortion. With increasing of irradiation dose, mechanism was proposed at different irradiation stage. In the case of 10^{15} ions/cm^2 irradiation, the main type of irradiation damage was considered as interstitial which exerted compression stress on surrounded crystals. Consequently, distance of diffraction planes was decreased by compression stress in the irradiation surface layer, leading to a bit right shift (0.14°) of diffraction peaks. On the other hand, target surface was cleaned with energetic ions bombardment which brought about high intensity of α-Al peaks. When irradiation dwell time was added to 136 s , number of vacancies increased with the increasing of irradiation dose.[27] Herein, helium was performed as cavity nucleation sites and then more vacancies, vacancy clusters and interstitial atoms were generated. In order to reduce lattice strain, vacancy clusters grow with absorbing additional vacancies.[28] Therefore, distortion generated by vacancy clusters is greater than interstitial, which produce a large tensile stress on surrounding crystal,[29] and lead to intensity decrease and left shift (0.2°) of peaks in the diffractogram. However, these vacancy clusters have a tendency to collapse and form

a mass of line defects.[30] Fig. 6 shows TEM images of 1060 pure aluminum without irradiation and with 10^{16} ions/cm^2 irradiation. In virgin sample, only a few dislocations (the density is about 1.8×10^{11}/cm^2) were observed, as shown in Fig. 6(a). However, high density of dislocations (the density is about 3.3×10^{11}/cm^2) presented in sample with 10^{16} ions/cm^2 irradiation, as illustrated Fig. 6(b).

During irradiation processing, most of the energy loss during collisions transformed into thermal energy. In comparison with ambient temperature, this results in a significantly high temperature (about 630 K, 10^{17} ions/cm^2 irradiation) of the target surface layer, which promote diffusion of vacancies and atoms, crystal lattice recovery,[31] helium-vacancy clusters growth,[32] and release stress concentration in irradiation sample surface layer. This suggests that diffraction pattern shift toward higher Bragg angles with 10^{17} ions/cm^2 ions irradiation. In addition, regularity variation of two peaks corresponding to (041), (624) planes of $Al_9Fe_2Si_2$ phase are consistent with peak variation of α-Al. Whereas, significant peak changes of (111) plane was also observed in Fig.5, indicating a decrease of organizational order of $Al_9Fe_2Si_2$ phase by increasing irradiation dose, and finally induced amorphization with 10^{17}ions/cm^2 irradiation.

4 Conclusions

Crystal defects, strain changes, phase transformation and morphology altered in 1060 pure aluminum surface layer introduced by helium irradiation are explored in this work. Sample surface morphologies are varied with helium irradiation and the

changes mainly appear in the form of pinholes and micro-cracks. These damages grow with increasing of irradiation dose. Mean roughness of sample surface increase with addition of irradiation dose and a peak value of 6.178 nm is obtained at 10^{17} ions/cm^2 irradiation. Meanwhile, strain variation presents in helium irradiation samples, and the degree of irradiation damage depends on the dosage of irradiation. With 10^{15} ions/cm^2 irradiation, predominant distortion was caused by interstitial, which present compression stress. However, in samples with 10^{16} ions/cm^2 irradiation, this was taken over by tensile stress which was mainly induced by vacancy clusters. In addition, the structure disorder of Al-Fe-Si phase is caused by helium irradiation, which is increased with addition of irradiation dose, and eventually leads to amorphization of Al-Fe-Si phase with 10^{17} ions/cm^2 irradiation.

ACKNOWLEDGMENTS

This work was supported by the National Natural Science Foundation of China (No. 51175238), the Industrial Supporting Plan of Zhenjiang City (No.GY2013011), "Six talent peaks" of high level talent selection and training project of Jiangsu Province (No. 2013-ZBZZ-031), and the Priority Academic Program Development of Jiangsu Higher Education Institutions. The authors would like to thank Jian Chuan Ming, from *Chang Zhou Bo Rui Heng Electronic Technology Co., Ltd* for his technical direction. Rui Zhang, Zheng Dong Wu and Yu Shan Li from Jiangsu University are appreciated for sample preparation.

Reference

1. P. Romero-Gomez, A. Palmero, T.Ben, J. G. Lozano, S. I. Molina, and A. R. González-Elipe.

Phys. Res. B. **115420**, 82(2010)

2. N. Yoshida, H. Iwakiri, K. Tokunaga, and T. Baba. J. Nucl. Mater. **946**, 337(2005).

3. N. J. Dutta, N. Buzarbaruah, and S. R. Mohanty. J. Nucl. Mater. **51**, 452(2014).

4. T. J. Kang, T. Kim, S. Park, J. S. Lee, J. H. Lee, J. Hahn, H. Lee, and Y. H. Kim. Sensor. Actuat A-Phys. **116**, 216(2014)

5. J. Chen, P. Jung, T. Rebac, F. Duval, T. Sauvage, Y. de Carlan, and M. F. Barthe. J. Nucl. Mater. **253**, 453(2014).

6. T. Miura, K. Fujii, and K. Fukuya. J. Nucl. Mater. **279**, 457(2015).

7. N. Li, N. A. Mara, Y. Q. Wang, M. Nastasi, and A. Misra. Scripta. Mater.**64**, 974 (2011)

8. B. Cui, J. Kacher, M. McMurtrey, G. Was, and I. M. Robertson. Acta. Mater. **65**, 150(2014)

9. Z. Aabdin, N. Peranio, and O. Eibl. Adv. Mater. **24**, 4605(2012)

10. Y. J. Xiao, F. Z. Fang, Z. W. Xu, W. Wu, and X. C. Shen. Nucl. Instrum. Meth. B. **253**, 307(2013)

11. D. Kiener, P. Hosemann, S. A. Maloy, and A. M. Minor. Nat. Mater. **608**, 10(2011)

12. P. Romero-Gomez, A. Palmero, F. Yubero, M. Vinnichenko, A. Kolitsch, and A. R. Gonzalez-Elipe. Scripta. Mater. **574**, 60 (2009)

13. R. Callec, P. N. Favennec, M. Salvi, H. L'Haridon, and M. Gauneau. J. Appl. Phys. **1872**, 59(1991)

14. S. M. Myers, D. M. Follstaedt, G. A. Petersen, C. H. Seager, H. J. Stein, and W. R. Wampler. Nucl. Instrum. Meth. B. **379**, 106(1995)

15. C. Li, L. R. Zhao, Y. F. Mao, W. G. Wu, and J. Xu. Sci. Rep. **5**, 8236(2015).

16. D. Perrone, R. O. Dendy, I. Furno, R. Sanchez, G. Zimbardo, A. Bovet, A. Fasoli, K.

Gustafson, S. Perri, P. Ricci, and F. Valentini. Space Sci. Rev. **233**, 178(2013)

17. J. H. Adams, Jr., R. Silberberg, and C. H. Tsao. NRL Memorandum Report 4506. August 25, 1981
18. R. Figueroa, C. M. Abreu, M. J. Cristóbal, and G. Pena. Wear. **53**, 276-277(2012)
19. T. Mitsuda, I. Kobayashi, S. Kosugi, Nao. Fujita, Y. Saitoh, F. Hori, S. Semboshi, Y. Kaneno, K. Nishida, N. Soneda, S. Ishino, A. Iwase. Nucl. Instrum. Meth. B. **49**, 272(2012)
20. S. Thibault, and E. Hug. Applied surface science. **311**, 310(2014)
21. S. Morito, , J. Nishikawa, and T. Maki. ISIJ. Int. **1475**, 43(2003)
22. http://www.srim.org/
23. I. V. Afanasyev-Charkin, K. E. Sickafus. J. Nucl. Mater. **112**, 306(2002).
24. W. Khalifa, F. H. Samuel, and J. E. Gruzleski. Metall. Mater. Trans. A, **807**, 34A(2003)
25. K. E. Sickafus, R. W. Grimes, J. A. Valdes, A. Cleave, M. Tang, M. Ishimaru, S. M. Corish, C. R. Stanek, and B. P. Uberuage. Nat. Mater. **217**, 6(2007)
26. M.M. Silva, L. Pichon, M. Drouet, and J. Otubo. Surf. Coat. Tech. **209**, 211(2012)
27. H. Zhang, Z. W. Yao, M. R. Daymond, and M. A. Kirk. J. Appl. Phys. **115**, 103508(2014)
28. D. Terentyev, N. Anento, A Serra, C. J. Ortiz, and E. E. Zhuikin. J. Nucl. Mater. **11**, 458(2014)
29. K. Nordlund, J. Keinonen, M. Ghaly, and R. S. Averback. Nature **49-51**, 398(1999).
30. H. Zhang, Z. W. Yao and M. R. Daymond, and M. A. Kirk. J. Appl. Phys. **115**, 103509(2014)
31. J. C. Nappé, I. Monnet, Ph. Grosseau, F. Audubert, B. Guilhot, M. Beauvy, M. Benabdesselam, and L. Thomé. J. Nucl. Mater. **53**, 409(2011).
32. F. F. Luo, L. P. Guo, J. C. Chen, T. C. Li, Z. C. Zheng, Z. Yao, J. P. Suo. J. Nucl. Mater. **339**,

455(2014).

Captions of tables

Table 1 chemical composition of 1060 aluminum alloy (wt%)

Fe	Si	Cu	Zn	V	Mn	Ti	Mg	Al
0.35	0.25	0.05	0.05	0.05	0.03	0.03	0.03	Balance

Table 2 Energy loss of incident ions in target calculate by SRIM-2008 for a helium ion beam of 50 keV energy (%)

Energy loss	Ionization	Vacancies	Phonons
Ions	44.31	0.13	0.44
Recoils	23.77	2.51	28.85

Captions of figures

Fig. 1. Schematic diagrams of home-made MT3-R ion implanter

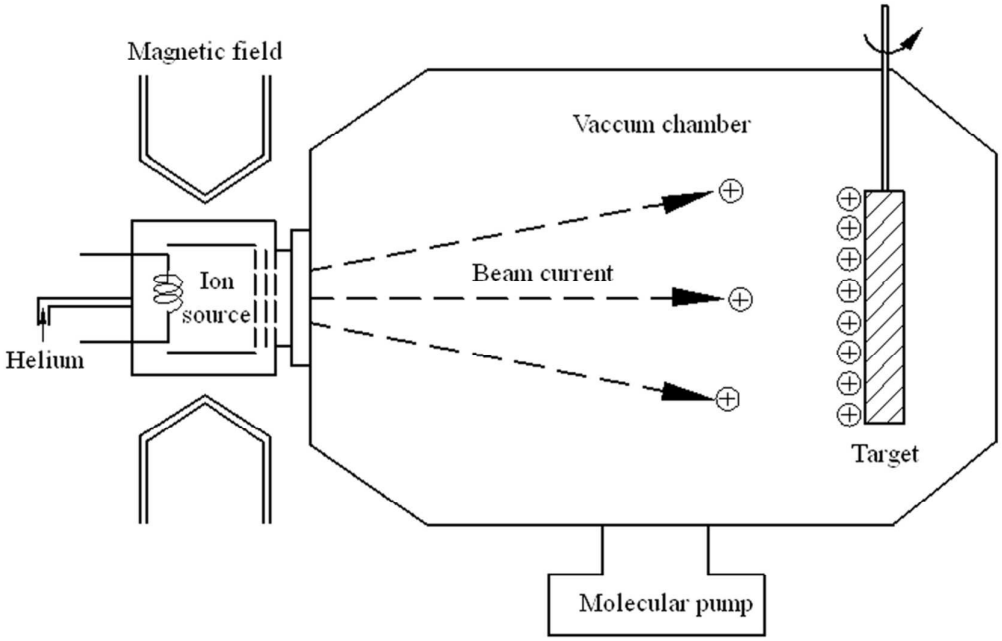

Fig. 2. Collision events calculated by SRIM-2008 of Helium irradiation (50keV)

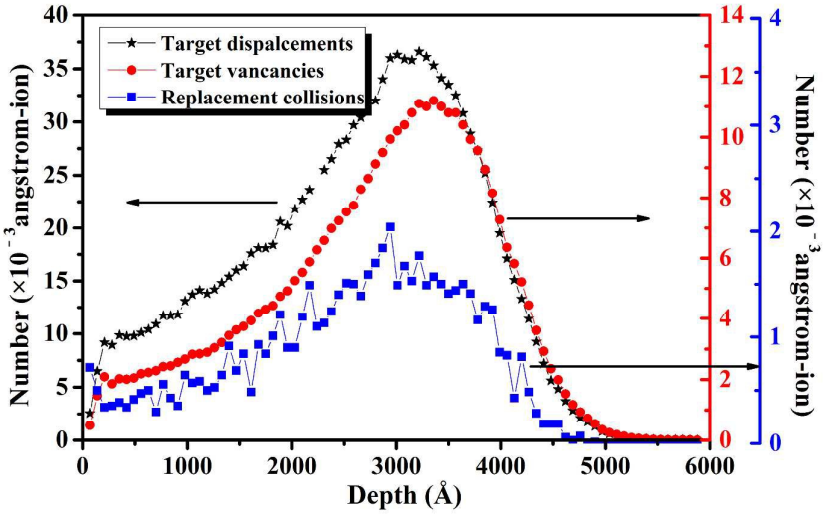

Fig. 3. SEM images of specimens (a) Reference, (b) 10^{15} ions/cm^2, (b) 10^{16} ions/cm^2, (c) 10^{17} ions/cm^2

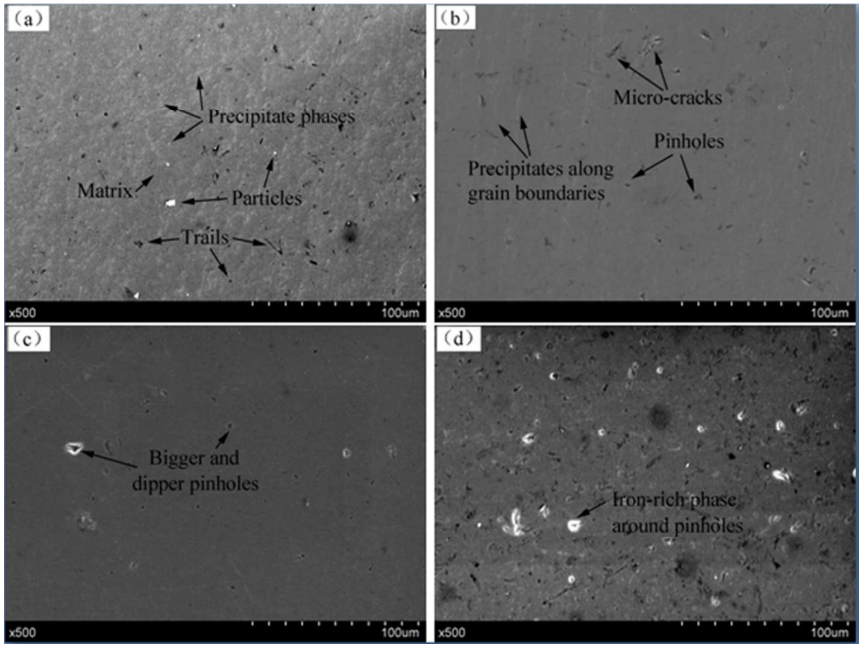

Fig. 4. Average, maximum and minimum roughness of sample surfaces

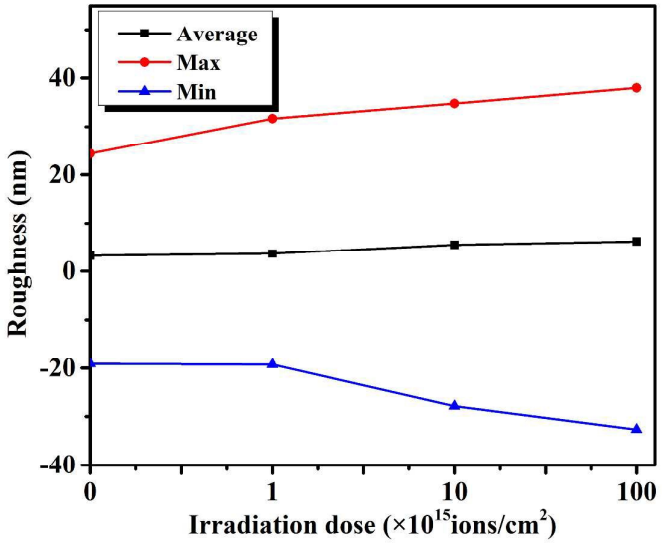

Fig. 5. X-ray diffraction patterns of reference and irradiation samples

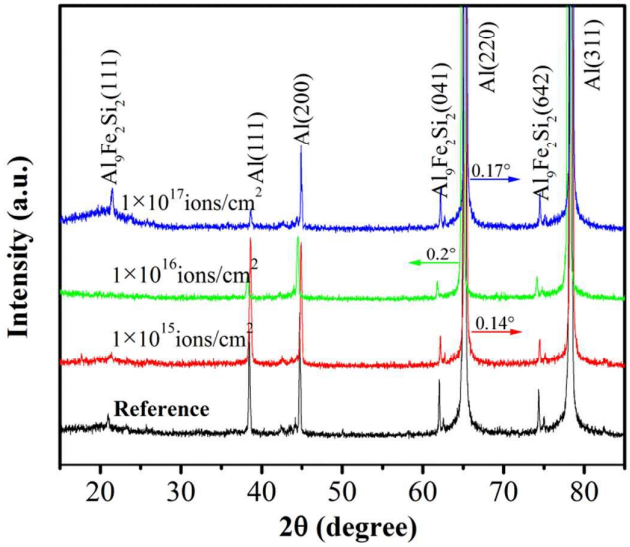

Fig. 6. TEM images of 1060 aluminum: (a) virgin sample; (b) 10^{16} ions/cm^2 irradiation